



Quantum speed limit via the trajectory ensemble

Xianghong Hu (胡相虹), Shuning Sun (孙舒宁), and Yujun Zheng (郑雨军) ^{*}
School of Physics, Shandong University, Jinan 250100, China

 (Received 10 October 2019; accepted 10 March 2020; published 13 April 2020)

In this paper, we present the theoretical framework of quantum speed limits (QSLs) in terms of trajectory ensembles in phase space. This indicates that the QSL can be thought of as the summation of the connecting harmonic oscillators: the connections between the points of the system in phase space and the trajectory ensemble. Two typical models, the time-dependent harmonic oscillator and the undriven harmonic oscillator coupled to a thermal bath, are investigated by employing the theoretical framework. Our results from this perspective are in agreement with previous treatments.

DOI: [10.1103/PhysRevA.101.042107](https://doi.org/10.1103/PhysRevA.101.042107)

I. INTRODUCTION

Quantum speed limits (QSLs) provide the lower bounds on the evolution time between two distinguishable states of a quantum system. QSLs have potential applications in quantifying and controlling quantum coherence and protecting quantum information from decoherence caused by environmental noise [1]. QSLs offer limits to parameter estimation in quantum metrology [2], the computational capability of physical devices [3], and information scrambling [4]. Originally, the QSL was considered as an interpretation of Heisenberg indeterminacy. The explanation stems from the Mandelstam and Tamm bound (MT bound) [5] in terms of unitary processes, which estimates the speed of evolution from the perspective of energy dispersion of the initial state. Margolus and Levitin established another bound (ML bound) for unitary dynamics [6]. The ML bound is related to the difference between the mean energy and the ground-state energy. It has been shown that the unified bound of MT and ML bounds is tight [7].

The interaction between a quantum system and its environment is generally unavoidable, and so QSLs beyond unitary dynamics have been investigated [8–11]. For open quantum systems, the effects of the interactions between the quantum system and its environment on QSL have been widely investigated in the context of non-Markovianity [12–16], the entanglement of quantum systems, and other situations [17–20]. Both equilibrium and nonequilibrium environmental effects on QSLs for open quantum systems have been investigated [16,18]. QSLs for leakage, decoherence, and experimental measurement have also been addressed [21,22]. Further, different metric measures have been employed in the investigation of QSLs, for example, the relative purity, trace distance, and even a whole family of contractive Riemannian metrics [8–10,16,23].

In addition to the MT and ML bounds, a distinct bound which relates QSLs to the geometric phase has been suggested. The relation between QSLs and the Pancharatnam connection 1-form has been established based on the

gauge-invariant distance in the Riemannian metric, which shows the potential possibilities for speedup of the holonomy quantum computation [24].

It was shown previously that a speed limit can exist for both quantum and classical systems [25,26], which leads to some interesting questions. For example, what are the contributions of classical partitions to the QSLs? Can we understand the differences between QSLs and classical speed limits by comparing classical and quantum dynamics in phase space? How does the evolving status of the system influence quantum and classical speed limits?

The Wigner representation of quantum mechanics can be employed effectively to study these questions [26–30]. The Wigner function is a faithful and exact representation of quantum mechanics in phase space and has been widely applied in the description and analysis of quantum problems [30]. In the resulting quantum phase space, the qualitative nature of quantum mechanics can be captured and visualized through vivid classical-like physical pictures [29,30]. Some interesting questions can be investigated in terms of the Wigner function, such as the behavior of QSLs across the quantum-to-classical transition, the measurement of the Chern number via Wigner function flux, the measurement of cat states, entanglement dynamics, fractional Lévy flight, quantum tunneling, and other manifest quantum processes [26–28,31–35]. In this context, it was recently shown that a single trajectory of a quantum system can evolve from an initial to a distinguishable state at velocities exceeding the QSL [36].

In this paper, we present a description of the QSL in terms of trajectory ensembles via the Wigner representation of quantum mechanics in phase space. In the context of the trajectory ensemble, we find that the QSL can be understood from the perspective of the i th connecting harmonic oscillator (CHO- i), which is the Hamiltonian of the scaled harmonic oscillator. CHO- i connects the position Γ of the system in phase space with the i th trajectory in the trajectory ensemble. This provides us with a unique perspective: the QSL is the summation of the average of energy flux of the CHO over all of the phase space. In addition, it illustrates that two factors will affect QSLs: the time changes of CHO and its corresponding partitions.

^{*}yzheng@sdu.edu.cn

This paper is organized as follows. In Sec. II, we present the equation of motion of the trajectory ensemble and derive an expression of the quantum speed limit in terms of the trajectory ensemble evolution. In Sec. III, we show the numerical results of QSLs for two models: the time-dependent harmonic oscillator and an undriven harmonic oscillator coupled to a thermal bath. Also, we investigate the contributions of the trajectories in the ensemble to the QSL and the corresponding nature of the trajectories. In Sec. IV, we give a discussion and conclusions.

II. THEORETICAL FRAMEWORK

To investigate QSLs in phase space via the trajectory ensemble, we employ the phase-space representation of quantum mechanics: the Wigner representation [29,30].

A. QSL using the Wigner function

The Wigner function in phase space is, corresponding to the density operator $\rho_t = \rho(t)$, defined as follows [30]:

$$W(q, p; t) = \frac{1}{2\pi\hbar} \int_{-\infty}^{\infty} d\xi e^{-\frac{i p \xi}{\hbar}} \left\langle q + \frac{1}{2}\xi | \rho(t) | q - \frac{1}{2}\xi \right\rangle \equiv W(\Gamma, t), \quad (1)$$

where the phase-space coordinates are denoted $\Gamma = (q, p)$.

QSLs have been investigated widely by employing a family of contractive Riemannian metrics [37] to measure the distance between two distinguishable states, such as relative purity, trace distance, etc. [8,16,23].

The distance between distinguishable states can be quantified using the trace distance as the case $p = 1$ of the Schatten p -norm,

$$\begin{aligned} \ell_p(\rho_t, \rho_0) &= \|\rho_t - \rho_0\|_p \\ &= (\text{tr}\{|\rho_t - \rho_0|^p\})^{\frac{1}{p}}, \end{aligned} \quad (2)$$

namely, $\ell_1(\rho_t, \rho_0) = \text{tr}\{|\rho_t - \rho_0|\}$. QSLs were studied previously using the trace norm [16,28]. Correspondingly, using the Wigner function representation of quantum mechanics in phase space, we employ the Wasserstein 1-distance as a measure of the distance $\mathcal{D}(t)$, i.e., the distinguishability of the states,

$$\begin{aligned} \mathcal{D}(t) &= \|W(\Gamma, t) - W(\Gamma, 0)\|_1 \\ &= \int d\Gamma |W(\Gamma, t) - W(\Gamma, 0)|. \end{aligned} \quad (3)$$

By using the triangle inequality, we have

$$\dot{\mathcal{D}}(t) \leq |\dot{\mathcal{D}}(t)| \leq \int d\Gamma |\dot{W}(\Gamma, t)|, \quad (4)$$

where

$$\begin{aligned} \dot{\mathcal{D}}(t) &\equiv \frac{d}{dt} \mathcal{D}(t) \\ &= \int d\Gamma \frac{W(\Gamma, t) - W(\Gamma, 0)}{|W(\Gamma, t) - W(\Gamma, 0)|} \dot{W}(\Gamma, t). \end{aligned} \quad (5)$$

Finally, the QSL in phase space can be defined as

$$v_{\text{QSL}}^W \equiv \|\dot{W}(\Gamma, t)\|_1 = \int d\Gamma |\dot{W}(\Gamma, t)|. \quad (6)$$

Deffner noted that the expression of Eq. (6) has the same functional form as the expression of the QSL in density operator space but is significantly easier to compute [28].

B. Entangled trajectory dynamics

To calculate the value of the expression of Eq. (6), we should evolve the Wigner function in phase space. The evolution equation of the Wigner function is [30]

$$\frac{\partial W(\Gamma, t)}{\partial t} = -\frac{p}{m} \frac{\partial W(\Gamma, t)}{\partial q} + \int d\xi J(q, \xi - p) W(q, \xi; t), \quad (7)$$

where

$$J(q, \xi) = \frac{i}{2\pi\hbar^2} \int dz \left[V\left(q + \frac{z}{2}\right) - V\left(q - \frac{z}{2}\right) \right] e^{-\frac{i}{\hbar} z \cdot \xi} \quad (8)$$

and $V(q)$ is the potential energy of the system.

The evolution equation of the Wigner function of Eq. (7) can also be expressed as the form of the continuity equation

$$\frac{\partial W(\Gamma, t)}{\partial t} + \nabla \cdot \mathbf{j}(\Gamma, t) = 0, \quad (9)$$

where $\mathbf{j}(\Gamma, t)$ is the flux vector in the phase space, which is defined as

$$\mathbf{j}(\Gamma, t) = (\dot{q}, \dot{p}) W(\Gamma, t). \quad (10)$$

Correspondingly, we have

$$\nabla \cdot \mathbf{j}(\Gamma, t) = \frac{\partial}{\partial q} [\dot{q} W(\Gamma, t)] + \frac{\partial}{\partial p} [\dot{p} W(\Gamma, t)]. \quad (11)$$

Then,

$$\frac{\partial W(\Gamma, t)}{\partial t} = -\frac{\partial}{\partial q} [\dot{q} W(\Gamma, t)] - \frac{\partial}{\partial p} [\dot{p} W(\Gamma, t)]. \quad (12)$$

By comparing Eqs. (7) and (12), we obtain the equations of motion for the entangled trajectories of the system [31,38,39]:

$$\dot{q} = \frac{p}{m}, \quad (13)$$

$$\dot{p} = -\frac{1}{W(q, p)} \int \Theta(q, \xi - p) W(q, \xi) d\xi,$$

where

$$\Theta(q, \eta) = \frac{1}{2\pi\hbar} \int_{-\infty}^{\infty} \left[V\left(q + \frac{y}{2}\right) - V\left(q - \frac{y}{2}\right) \right] \frac{e^{-i\eta y/\hbar}}{y} dy. \quad (14)$$

There have been a number of methods proposed to propagate the quantum system and Wigner function using the evolution of trajectory ensembles [31,38–46]. As one of these methods, the entangled trajectory equations of Eq. (13) have been employed to investigate entanglement dynamics, H_2O photodissociation, fractional Lévy flight, tunneling time in a driven double-well system, quantum tunneling in multidimensional systems, etc. [32,33,39,46–50].

C. QSLs using the entangled trajectory method

The above section suggests that the Wigner function can be estimated from a long trajectory $\Gamma(t)$ in phase space over the observation time τ . In particular, the Wigner function can be understood by employing the fraction of time Δt the trajectory spends in the position Γ in phase space via the time series $\{\Gamma(\Delta t), \Gamma(2\Delta t), \Gamma(3\Delta t), \dots\}$. There exists a range of possible methods to construct the Wigner function from a finite set of N sampled points. In this paper, we employ a kernel approach [51,52] to estimate the Wigner function from a sampling by a trajectory ensemble. The Wigner function is then given by

$$W(\Gamma, t) = \frac{1}{N} \sum_{i=1}^N \frac{1}{h^f} K\left(\frac{\Gamma - \Gamma_i(t)}{h}\right), \quad (15)$$

where $K(\cdot)$ is the kernel function, $N = \tau/\Delta t$, f is the dimension of the system, and $h = \{4/[N(f+2)]\}^{1/(f+4)}$ is the kernel window width [52]. The i th trajectory $\Gamma_i(t) \equiv (q_i(t), p_i(t))$ is a member of the ensemble of trajectories in phase space.

In our following numerical kernel estimation, we place a Gaussian at the position Γ in phase space by choosing the Gaussian kernel

$$K(\Gamma) = \frac{1}{2\pi\sigma_p\sigma_q} e^{-\frac{p^2}{2\sigma_p^2} - \frac{q^2}{2\sigma_q^2}}, \quad (16)$$

where σ_q and σ_p obey the minimum uncertainty relation between the canonical variables q and p .

Based on Eqs. (15) and (16), we obtain

$$\begin{aligned} W(\Gamma, t) &= \frac{1}{N} \sum_{i=1}^N \frac{1}{2\pi h_p h_q} e^{-\frac{[p-p_i(t)]^2}{2h_p^2} - \frac{[q-q_i(t)]^2}{2h_q^2}} \\ &\equiv \frac{1}{N} \sum_{i=1}^N K_i(\Gamma, t), \end{aligned} \quad (17)$$

with $h_p = h\sigma_p$ and $h_q = h\sigma_q$.

The time derivative of the Wigner function becomes

$$\begin{aligned} \dot{W}(\Gamma, t) &= \frac{1}{N} \sum_{i=1}^N \dot{K}_i(\Gamma, t) \\ &= \frac{1}{N} \sum_{i=1}^N \left[\frac{\partial K_i(\Gamma, t)}{\partial q_i} \dot{q}_i(t) + \frac{\partial K_i(\Gamma, t)}{\partial p_i} \dot{p}_i(t) \right]. \end{aligned} \quad (18)$$

Let $\Delta q_i(t) = q - q_i(t)$ and $\Delta p_i(t) = p - p_i(t)$. Hence, $\Delta \Gamma_i(t) = \Gamma - \Gamma_i(t) = (\Delta q_i(t), \Delta p_i(t))$ are the differences between the position Γ in phase space and the i th trajectory $\Gamma_i(t) \equiv (q_i(t), p_i(t))$. By using

$$\begin{aligned} \frac{\partial K_i(\Gamma, t)}{\partial q_i} &= K_i(\Gamma, t) \frac{\Delta q_i}{h_q^2}, \\ \frac{\partial K_i(\Gamma, t)}{\partial p_i} &= K_i(\Gamma, t) \frac{\Delta p_i}{h_p^2}, \end{aligned} \quad (19)$$

and

$$\dot{q}_i = -\Delta \dot{q}_i, \quad \dot{p}_i = -\Delta \dot{p}_i, \quad (20)$$

Eq. (18) can be written as

$$\dot{W}(\Gamma, t) = -\frac{1}{N} \sum_{i=1}^N K_i(\Gamma, t) \left(\frac{\Delta q_i}{h_q} \frac{\Delta \dot{q}_i}{h_q} + \frac{\Delta p_i}{h_p} \frac{\Delta \dot{p}_i}{h_p} \right). \quad (21)$$

For convenience, we introduce the scaled canonical coordinates and momenta, namely, $q/h_q \rightarrow q$ and $p/h_p \rightarrow p$. Equation (21) can be rewritten as follows:

$$\begin{aligned} \dot{W}(\Gamma, t) &= -\frac{1}{N} \sum_{k=1}^N K_i(\Gamma, t) (\Delta q_i \Delta \dot{q}_i + \Delta p_i \Delta \dot{p}_i) \\ &= -\frac{1}{N} \sum_{i=1}^N K_i(\Gamma, t) \frac{d}{dt} \left(\frac{\Delta q_i^2 + \Delta p_i^2}{2} \right) \\ &\equiv -\frac{1}{N} \sum_{i=1}^N \dot{\varepsilon}_i K_i(\Gamma, t), \end{aligned} \quad (22)$$

where we let

$$\varepsilon_i = \frac{1}{2} (\Delta q_i^2 + \Delta p_i^2). \quad (23)$$

ε_i can be considered to be the Hamiltonian of the scaled harmonic oscillator connecting the position Γ of the system with the i th trajectory in phase space. ε_i can therefore be denoted as CHO- i . Physically, Eq. (22) presents the time change of the Wigner function in phase space Γ at time t as the ensemble average of the trajectory over the time changes of CHO with its partition $K_i(\Gamma, t)$. Since $\dot{\varepsilon}_i$ are the time changes of CHO energy and $K_i(\Gamma, t)$ are the corresponding partitions, $\dot{\varepsilon}_i K_i(\Gamma, t)$ can also be thought of as the energy flux of CHO- i . Therefore, Eq. (22) states that the time changes of the Wigner function can be thought of as the average of the energy flux of the CHO of the system over the trajectory ensemble in the position of phase space Γ at time t .

We define

$$\bar{J}(\Gamma, t) = \left| \frac{1}{N} \sum_{i=1}^N \dot{\varepsilon}_i K_i(\Gamma, t) \right| \quad (24)$$

as the average of the energy flux of the CHO in phase-space point Γ at time t . We therefore arrive at an expression of the QSL by employing Eq. (24) in phase space,

$$v_{\text{QSL}}^E(t) = \int_{-\infty}^{\infty} \bar{J}(\Gamma, t) d\Gamma. \quad (25)$$

Expression (25) indicates that the QSL is the summation of the average of the energy flux of the CHO all over the phase space. By considering Eq. (24) we see that there are two factors that influence the QSL: the time changes in the energy of the CHO [Eq. (23)] and their corresponding partitions $K_i(\Gamma, t)$.

III. NUMERICAL RESULTS

In this section we show the numerical results for two typical models: the time-dependent harmonic oscillator, which served as the Paul trap model, and an undriven harmonic oscillator coupled to a thermal bath.

A. The time-dependent harmonic oscillator

We first consider the time-dependent harmonic oscillator,

$$H = \frac{1}{2m}\hat{p}^2 + \frac{1}{2}m\omega^2(t)\hat{q}^2, \quad (26)$$

where the time-dependent frequency is taken from Ref. [28]: $\omega^2(t) = \omega_2^2 - (\omega_2^2 - \omega_1^2)t/\tau$. The time-dependent harmonic oscillator has been used as the Paul trap model [30]. Also, investigations of the QSL for the system have been reported, such as the comparison of QSLs between the expressions of the density matrix and the Wigner function, across the quantum-to-classical transition [26,28].

In our numerical calculations, we choose the initial distribution to be a Gaussian,

$$W(\Gamma, 0) = \frac{1}{\pi\hbar} e^{-2aq^2 - \frac{1}{2\hbar^2 a} p^2}, \quad (27)$$

where $a = \frac{m\omega_2}{2\hbar}$.

For the system of Eq. (26), the entangled trajectory equations of motion from Eq. (13) can be written as follows:

$$\begin{aligned} \dot{q} &= \frac{p}{m}, \\ \dot{p} &= -m\omega^2(t)q. \end{aligned} \quad (28)$$

By employing the equations of motion (28) and (17), we can calculate the Wigner function expressed in terms of the ensemble of trajectories. In the case of the harmonic oscillator, we can obtain the expression of the Wigner function exactly using the trajectories. In particular, the expression of the Wigner function of Eqs. (28) and (17) in terms of the trajectory ensemble is equivalent to the following expression in Ref. [30]:

$$W(q, p, t) = W_0(q_0(q, p, t), p_0(q, p, t)), \quad (29)$$

where $W_0(q, p)$ is the Wigner function at time $t = 0$ and $(q_0(q, p, t), p_0(q, p, t))$ are the initial coordinates and momenta in phase space.

In our numerical calculations, we employ the trajectory ensemble to express the Wigner function.

In Fig. 1, we present the results for the QSL expressed via Eq. (25). To make a comparison with previous results, we employ the same parameters as used in Ref. [28], which are given in the caption of Fig. 1. In Fig. 1(a), we show the results for the total evolution time $\tau = 1$, while in Fig. 1(b) we give those for $\tau = 5$. We can find that the v_{QSL}^E results of Eq. (25) are the same as the results in Ref. [28]. We can see that when evolution time $\tau = 1$, v_{QSL} increases over time. And when evolution time $\tau = 5$, v_{QSL} has apparent oscillations with time.

To understand the behavior of QSLs, in Fig. 2 we show the distributions of the average energy flux of the CHO $\bar{j}(\Gamma, t)$ in phase space. We show snapshots of $\bar{j}(\Gamma, t)$ at time $t/\tau = 0.258, 0.46, 0.664$, and 0.826 for the case of $\tau = 5$. They correspond to the first four local maximum and minimum values of the QSL in Fig. 1(b).

From Fig. 2, we find that the oscillations of the QSL shown in Fig. 1(b) correspond to the rotations of the average energy flux $\bar{j}(\Gamma, t)$ of the system in phase space. This originates from the nature of the quantum system, namely, the time-dependent

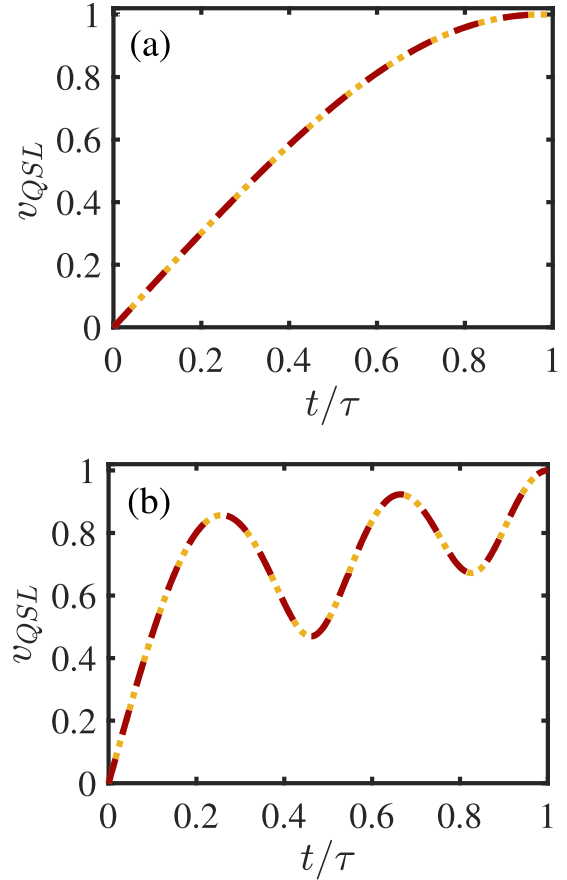


FIG. 1. Quantum speed limit v_{QSL}^E and v_{QSL}^W normalized by their maximal values during the time interval $t \in [0, \tau]$ for the time-dependent harmonic oscillator. v_{QSL}^W , denoted by the dotted orange (light gray) line, is obtained using the direct Wigner function $W(q, p, t)$ in Ref. [28]. v_{QSL}^E , denoted by the dashed red (dark gray) line, is obtained using the trajectory method in the work. Parameters are taken from Ref. [28]: $\omega_2 = 1, \omega_1 = 2, m = 1, \hbar = 1$, and (a) $\tau = 1$ or (b) $\tau = 5$. The units are arbitrary.

harmonic oscillator. It is interesting that the average energy flux $\bar{j}(\Gamma, t)$ has “zero” lines in phase space, as shown in Fig. 2. We attribute the zero lines to be the result of the superposition of the energy flux of CHO- $i \dot{\varepsilon}_i K_i(\Gamma, t)$ since ε_i could increase or decrease in the evolution.

B. The undriven harmonic oscillator coupled to a thermal bath

In this section, we consider an undriven harmonic oscillator with potential $V(q) = \frac{1}{2}m\omega_0^2 q^2$ coupled to a thermal bath. The dynamics of the undriven harmonic oscillator can be described via the following master equation [53]:

$$\partial_t W(\Gamma, t) = \mathcal{L}(\Gamma)W(\Gamma, t), \quad (30)$$

where

$$\mathcal{L}(\Gamma) = -\frac{p}{m}\partial_q + V'(q)\partial_p + \partial_p(\gamma p + D_{pp}\partial_p) + D_{qp}\partial_{qp}^2, \quad (31)$$

and its corresponding coefficients are $D_{pp} = m\gamma/\beta + m\beta\gamma\hbar^2(\omega_0^2 - \gamma^2)/12$ and $D_{qp} = \beta\gamma\hbar^2/12$, where γ is the

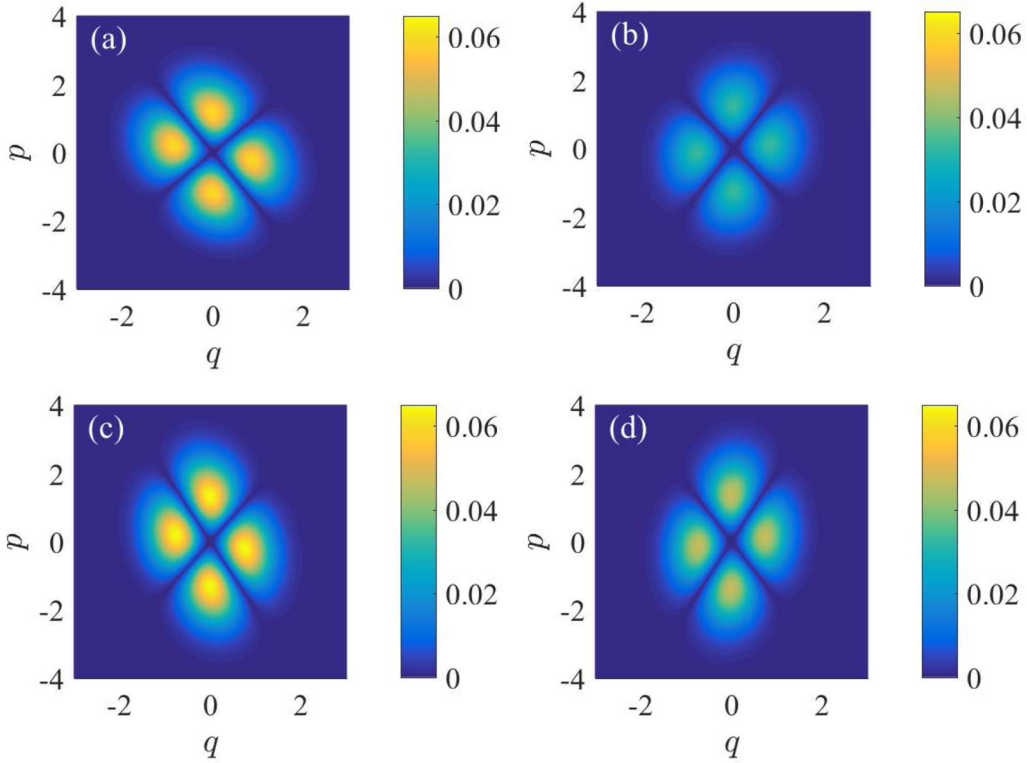


FIG. 2. Snapshots of the average energy flux of CHO $\bar{J}(\Gamma, t)$ with the parameters of Fig. 1 for the case of $\tau = 5$. (a)–(d) correspond to $t = 1.29, t = 2.30, t = 3.32$, and $t = 4.13$, respectively.

friction coefficient, $\beta = 1/(k_B T)$, k_B is Boltzmann constant, and T is the temperature.

By using Eqs. (13), (30), and (31), we can get the equations of motion for the entangled trajectories

$$\begin{aligned} \dot{q} &= \frac{p}{m} - D_{qp} \frac{1}{W(\Gamma, t)} \frac{\partial W(\Gamma, t)}{\partial p}, \\ \dot{p} &= -V'(q) - \gamma p - D_{pp} \frac{1}{W(\Gamma, t)} \frac{\partial W(\Gamma, t)}{\partial p}. \end{aligned} \quad (32)$$

In the following numerical calculations, the initial distribution is chosen to be the Gaussian distribution employed in Ref. [28],

$$W(\Gamma, t = 0) = \frac{1}{2\pi\sigma_q\sigma_p} e^{-\frac{(q-\mu_q)^2}{2\sigma_q^2} - \frac{(p-\mu_p)^2}{2\sigma_p^2}}. \quad (33)$$

In Fig. 3, we show the results of the QSL expressed via Eq. (25) using $1156 = 34 \times 34$ trajectories in the trajectory ensemble. To make a comparison, we also present the results of Ref. [28]. As shown in Fig. 3, the results of the QSL of Eq. (25) correspond well to the results of Ref. [28]. In addition, we find that v_{QSL} decreases over time generally. In the initial period, v_{QSL} declines rapidly, while later it falls slowly.

The distribution of the average flux of CHO $\bar{J}(\Gamma, t)$ in phase space at point Γ and time t shows us the vivid physical picture needed to understand QSL. Figure 4 shows that $\bar{J}(\Gamma, t)$ gets smaller as the evolution time passes for the dissipative system, which accounts for the decrease of v_{QSL}^E with the evolution time shown in Fig. 3. This indicates that the flux of the CHO goes to a steady state as the evolution time passes

as the energies of the system dissipate to the bath, causing the QSL to decay to a roughly constant value.

By analyzing the details of the motion of the trajectory ensemble in quantum phase space (shown in the Appendix), it can be seen that, when trajectories within a group have the same evolution direction generally, the rate summation

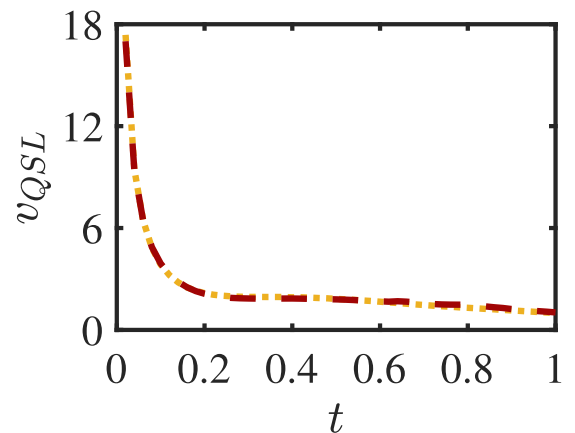


FIG. 3. Quantum speed limits v_{QSL}^W and v_{QSL}^E for the undriven harmonic oscillator coupled to a thermal bath with potential $V(q) = \frac{1}{2}m\omega_0^2 q^2$. v_{QSL}^E , denoted by the dashed red (dark gray) line, is obtained using the entangled trajectory method, and v_{QSL}^W , denoted by the dotted orange (light gray) line, is obtained using the Wigner expression of Ref. [28]. Parameters are taken from Ref. [28]: $\gamma = 2$, $\beta = 0.1$, $\hbar = 1$, $m = 1$, $\omega_0 = 1$, $\mu_q = 2$, $\sigma_q = 0.5$, $\mu_p = 0$, and $\sigma_p = 0.5$. The units are arbitrary.

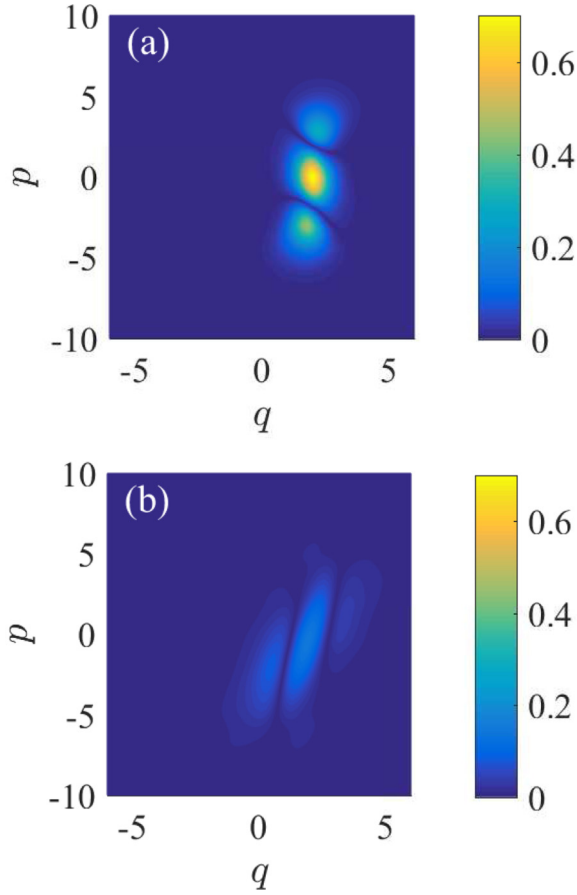


FIG. 4. The distributions of the average energy flux of CHO $\bar{J}(\Gamma, t)$ with the parameters of Fig. 3 for (a) $t = 0.1$ and (b) $t = 0.5$.

effect appears. Therefore, these trajectories contribute more partitions to v_{QSL} . In addition, we find that, from the perspective of the momentum dimension, the phase-space points located in the center part contribute less to the QSL compared to those away from the center in phase space. We attribute this to the differences in the time changes of CHO in different positions in phase space: for the dissipative system, the farther the trajectories are from the center of the phase space, the larger the time changes of the CHO are. This results in the correspondingly larger contributions to v_{QSL} .

IV. CONCLUSIONS AND DISCUSSION

In this paper, we presented the theoretical framework of the QSL in phase space using the entangled trajec-

tory formalism. We derived an expression of the quantum speed limit v_{QSL}^E using entangled trajectories and investigated v_{QSL}^E for two typical models. We showed that v_{QSL}^E obtained here is in agreement with the result of QSL obtained previously.

Our methodology indicates that QSL can be thought of as the superposition of the average energy flux of CHO over phase space: the time changes of the harmonic oscillators connecting the phase-space point Γ with the ensemble of trajectories with their corresponding partition $K_i(t)$. In particular, the expression of the QSL using the trajectory ensemble is given in Eq. (25). Therefore, the energy flux of the CHO and its partition would influence the QSL since the QSL is the “energy flux” of whole characteristics in phase space. This shows us the potential possibility of manipulating the QSL via changing the energy flux and/or its “partition.” In addition, we show that the contribution of different trajectory ensembles to v_{QSL}^E is variable. For a partial trajectory ensemble that evolves from the same momentum, the more consistent the velocity direction of these trajectories is, the greater the contribution this trajectory subset makes to the overall QSL. From another perspective, for the dissipative system, the farther the trajectories are from the center of phase space, the bigger the time changes of the CHO are. This results in correspondingly larger contributions to the QSL.

ACKNOWLEDGMENTS

X.H. thanks S. Deffner for fruitful discussions. The authors are indebted to Prof. C. Martens for carefully reading the manuscript. This work was supported by the National Basic Research Program of China (Grant No. 2015CB921004) and the National Natural Science Foundation of China (Grant No. 11674196).

APPENDIX: THE CONTRIBUTIONS OF DIFFERENT TRAJECTORY SUBSETS TO THE QSL

To understand the different contributions of different trajectories in the trajectory ensemble to the v_{QSL} of Eq. (25), we divide all trajectories into 34 groups. Each group of trajectories has the same momenta p_0 initially but different initial coordinates q_0 in phase space. Then we define the partial QSL v_{QSL}^p that is used to measure the contribution of involved trajectories to v_{QSL} as follows [see Eqs. (24)

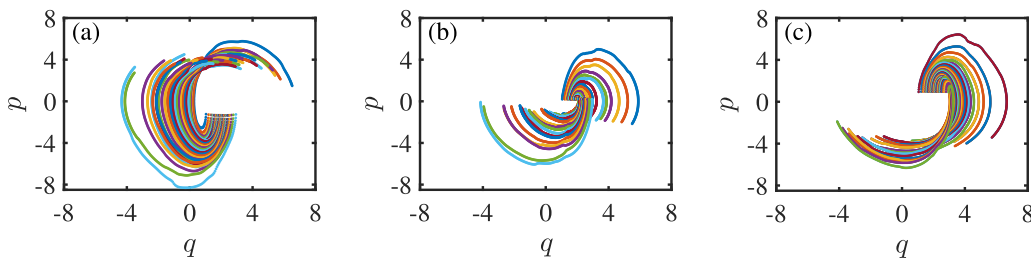


FIG. 5. The evolution of three kinds of typical trajectory subsets in phase space with the parameters of Fig. 3. Each trajectory subset has the same coordinate range but different momenta: (a) $p_0 = -0.7896$, (b) $p_0 = 0.1267$, and (c) $p_0 = 0.6020$.

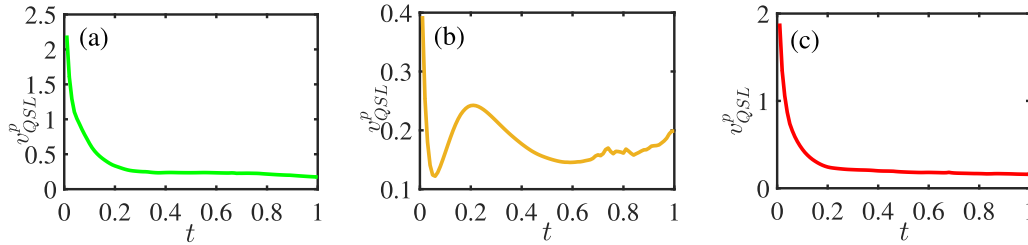


FIG. 6. The partial QSL v_{QSL}^p for three kinds of typical trajectory subsets corresponding to Fig. 5 with the parameters of Fig. 5.

and (25)]:

$$\begin{aligned}
 v_{\text{QSL}}^p(t) &= \int_{-\infty}^{\infty} \left| \frac{1}{N} \sum_{\kappa=N_0+1}^{N_0+n} J_{\kappa}(\Gamma, t) \right| d\Gamma \\
 &\equiv \int_{-\infty}^{\infty} \bar{J}^{p(n)}(\Gamma, t) d\Gamma, \quad (\text{A1})
 \end{aligned}$$

where the $(N_0 + 1)$ th trajectory is the first trajectory of each trajectory subset used in the paper.

To present the native properties, we take three groups of partial trajectories in the trajectory ensemble. We choose the initial momenta $p_0 = -0.7896$ in Fig. 5(a), the initial momenta $p_0 = 0.1267$ in Fig. 5(b), and the initial momenta $p_0 = 0.6020$ in Fig. 5(c). Note that Figs. 5(a) and 5(c) have a similar symmetry in phase space.

In Fig. 6, we show the results of v_{QSL}^p for the corresponding three groups of trajectories in Fig. 5. As shown in Fig. 6, although v_{QSL}^p shows trends similar to v_{QSL} , we find that the trajectories presented in Figs. 5(a) and 5(c) contribute significantly to v_{QSL}^E compared to those in Fig. 5(b).

Figure 5 shows the evolution of the three groups of trajectories in phase space. We can understand the different contributions of the three groups of trajectories to QSL by analyzing their evolution directions in phase space. As shown in Fig. 5, the trajectories of Fig. 5(a) have the same evolution direction generally, which illustrates the rate summation effect, and so do the trajectories in Fig. 5(c). However, in Fig. 5(b), the trajectories evolve towards two contrary directions initially, and there exists an offset between the velocity in different

directions, which shows a contrary effect compared to the aforementioned rate summation effect. This shows that we can attribute the magnitude of contributions to the relations of the evolution direction of trajectories which evolve from the same momentum.

To illustrate the contributions of the moving status of the trajectory subsets, we choose two groups of trajectories with the same initial coordinates and similar initial momenta but opposite directions; namely, in Fig. 5(a), we set the initial conditions as (q_0, p_0) , whereas in Fig. 5(c) the corresponding initial conditions are chosen as $(q_0, \sim -p_0)$. It is obvious that this quasisymmetry causes similar dynamics of the CHO- i in phase space for the two groups in Figs. 5(a) and 5(c). This leads to their similar contributions to v_{QSL} considering Eq. (A1), as shown in Figs. 6(a) and 6(c). However, as in the other case, we show the trajectory subset near the center of phase space in Fig. 5(b). For this case, the motion statuses of the trajectories present different behaviors, as shown in Fig. 6(b). Clearly, this indicates that they have different contributions to v_{QSL} .

From the above discussion, we know that from the perspective of momentum dimension, the phase-space points which are located in the center part contribute less to the quantum speed limit compared to those away from the center of phase space. We attribute this to the differences in the time changes of the CHO in different positions in phase space: for the dissipative system, the farther the trajectories are from the center of phase space, the bigger the time changes in the CHO are. This results in the larger contributions to v_{QSL} .

-
- [1] W. H. Zurek, *Rev. Mod. Phys.* **75**, 715 (2003).
 [2] M. Beau and A. del Campo, *Phys. Rev. Lett.* **119**, 010403 (2017).
 [3] V. Giovannetti, S. Lloyd, and L. Maccone, *Phys. Rev. A* **67**, 052109 (2003).
 [4] A. del Campo, J. Molina-Vilaplana, and J. Sonner, *Phys. Rev. D* **95**, 126008 (2017).
 [5] L. Mandelstam and I. Tamm, *J. Phys. (Moscow)* **9**, 249 (1945).
 [6] N. Margolus and L. B. Levitin, *Phys. D (Amsterdam, Neth.)* **120**, 188 (1998).
 [7] L. B. Levitin and T. Toffoli, *Phys. Rev. Lett.* **103**, 160502 (2009).
 [8] A. del Campo, I. L. Egusquiza, M. B. Plenio, and S. F. Huelga, *Phys. Rev. Lett.* **110**, 050403 (2013).
 [9] S. Deffner and E. Lutz, *Phys. Rev. Lett.* **111**, 010402 (2013).
 [10] M. M. Taddei, B. M. Escher, L. Davidovich, and R. L. de Matos Filho, *Phys. Rev. Lett.* **110**, 050402 (2013).
 [11] F. Campaioli, F. A. Pollock, F. C. Binder, and K. Modi, *Phys. Rev. Lett.* **120**, 060409 (2018).
 [12] X. Cai and Y. Zheng, *Phys. Rev. A* **94**, 042110 (2016).
 [13] X. Cai and Y. Zheng, *J. Chem. Phys.* **149**, 094107 (2018).
 [14] Y. J. Zhang, W. Han, Y. J. Xia, J. P. Cao, and H. Fan, *Phys. Rev. A* **91**, 032112 (2015).
 [15] H. B. Liu, W. L. Yang, J. H. An, and Z. Y. Xu, *Phys. Rev. A* **93**, 020105(R) (2016).
 [16] X. Cai and Y. Zheng, *Phys. Rev. A* **95**, 052104 (2017).
 [17] C. Liu, Z. Y. Xu, and S. Q. Zhu, *Phys. Rev. A* **91**, 022102 (2015).
 [18] Z.-Y. Xu, S. Luo, W. L. Yang, C. Liu, and S. Zhu, *Phys. Rev. A* **89**, 012307 (2014).

- [19] S. X. Wu, Y. Zhang, C. S. Yu, and H. S. Song, *J. Phys. A* **48**, 045301 (2015).
- [20] M. Bukov, D. Sels, and A. Polkovnikov, *Phys. Rev. X* **9**, 011034 (2019).
- [21] I. Marvian and D. A. Lidar, *Phys. Rev. Lett.* **115**, 210402 (2015).
- [22] D. Mondal and A. K. Pati, *Phys. Lett. A* **380**, 1395 (2016).
- [23] D. P. Pires, M. Cianciaruso, L. C. Céleri, G. Adesso, and D. O. Soares-Pinto, *Phys. Rev. X* **6**, 021031 (2016).
- [24] S. Sun and Y. Zheng, *Phys. Rev. Lett.* **123**, 180403 (2019).
- [25] M. Okuyama and M. Ohzeki, *Phys. Rev. Lett.* **120**, 070402 (2018).
- [26] B. Shanahan, A. Chenu, N. Margolus, and A. del Campo, *Phys. Rev. Lett.* **120**, 070401 (2018).
- [27] R. Uzdin and R. Kosloff, *Europhys. Lett.* **115**, 40003 (2016).
- [28] S. Deffner, *New J. Phys.* **19**, 103018 (2017).
- [29] F. E. J. Schroeck, *Quantum Mechanics on Phase Space* (Springer, Berlin, 1996).
- [30] W. P. Schleich, *Quantum Optics in Phase Space* (Wiley, Hoboken, NJ, 2011).
- [31] A. Donoso and C. C. Martens, *Phys. Rev. Lett.* **87**, 223202 (2001).
- [32] Z. Sun, H. Dong, and Y. Zheng, *Phys. Rev. E* **97**, 012132 (2018).
- [33] F. Xu, C. C. Martens, and Y. Zheng, *Phys. Rev. A* **96**, 022138 (2017).
- [34] T. Serikawa, J.-i. Yoshikawa, S. Takeda, H. Yonezawa, T. C. Ralph, E. H. Huntington, and A. Furusawa, *Phys. Rev. Lett.* **121**, 143602 (2018).
- [35] O. Steuernagel, D. Kakofengitis, and G. Ritter, *Phys. Rev. Lett.* **110**, 030401 (2013).
- [36] L. P. García-Pintos and A. del Campo, *New J. Phys.* **21**, 033012 (2019).
- [37] I. Bengtsson and K. Życzkowski, *Geometry of Quantum States: An Introduction to Quantum Entanglement* (Cambridge University Press, Cambridge, 2017).
- [38] A. Donoso, Y. Zheng, and C. C. Martens, *J. Chem. Phys.* **119**, 5010 (2003).
- [39] A. S. Wang, Y. Zheng, C. C. Martens, and W. Y. Ren, *Phys. Chem. Chem. Phys.* **11**, 1588 (2009).
- [40] A. Shimshovitz and D. J. Tannor, *Phys. Rev. Lett.* **109**, 070402 (2012).
- [41] X. Zhang and Y. Zheng, *Chin. Phys. Lett.* **26**, 023404 (2009).
- [42] E. J. Heller, *J. Chem. Phys.* **62**, 1544 (1975).
- [43] T. Dittrich, C. Viviescas, and L. Sandoval, *Phys. Rev. Lett.* **96**, 070403 (2006).
- [44] J. Cerrillo and J. Cao, *Phys. Rev. Lett.* **112**, 110401 (2014).
- [45] R. E. Wyatt, *Quantum Dynamics with Trajectories: Introduction to Quantum Hydrodynamics*, Interdisciplinary Applied Mathematics Vol. 28 (Springer, Berlin, 2006).
- [46] C. C. Martens, A. Donoso, and Y. Zheng, in *Quantum Trajectories*, edited by P. K. Chattaraj (CRC Press, Boca Raton, FL, 2016).
- [47] F. Xu, L. Wang, C. C. Martens, and Y. Zheng, *J. Chem. Phys.* **138**, 024103 (2013).
- [48] F. Xu, *Int. J. Quantum Chem.* **119**, 25854 (2019).
- [49] F. Xu, *Int. J. Quantum Chem.* **116**, 1057 (2016).
- [50] L. Wang, C. C. Martens, and Y. Zheng, *J. Chem. Phys.* **137**, 034113 (2012).
- [51] A. W. Bowman and A. Azzalini, *Applied Smoothing Techniques for Data Analysis: The Kernel Approach with S-Plus Illustrations*, Oxford Statistical Science Series Vol. 18 (Oxford University Press, Oxford, 1997).
- [52] B. W. Silverman, *Density Estimation for Statistics and Data Analysis* (Chapman & Hall/CRC, New York, 1998).
- [53] R. Dillenschneider and E. Lutz, *Phys. Rev. E* **80**, 042101 (2009).